Two-dimensional ferromagnetic extension of a topological insulator

P. Kagerer [1,2] C. I. Fornari [1,2,*] S. Buchberger [1,2] T. Tschirner,[2,3] L. Veyrat,[2,3,4] M. Kamp,[5] A. V. Tcakaev [2,4]
V. Zabolotnyy [2,4] S. L. Morelhão [6] B. Geldiyev,[1,2] S. Müller,[1,2] A. Fedorov,[2,3,7] E. Rienks,[7] P. Gargiani,[8] M. Valvidares,[8]
L. C. Folkers,[2,9] A. Isaeva [3,10] B. Büchner,[2,3] V. Hinkov [2,4] R. Claessen,[2,4] H. Bentmann [1,2,†] and F. Reinert [1,2]

[1]*Physikalisches Institut (EP7), Universität Würzburg, Am Hubland, D-97074 Würzburg, Germany*
[2]*Würzburg-Dresden Cluster of Excellence ct.qmat, Germany*
[3]*Leibniz IFW Dresden, Helmholtzstrasse 20, D-01069 Dresden, Germany*
[4]*Physikalisches Institut (EP4), Universität Würzburg, Am Hubland, D-97074 Würzburg, Germany*
[5]*Physikalisches Institut and Röntgen-Center for Complex Material Systems (RCCM), Fakultät für Physik und Astronomie,
Universität Würzburg, Am Hubland, D-97074 Würzburg, Germany*
[6]*Instituto de Física, Universidade de São Paulo, 05508-090 São Paulo, SP, Brazil*
[7]*Helmholtz-Zentrum Berlin für Materialien und Energie, Albert-Einstein-Strasse 15, D-12489 Berlin, Germany*
[8]*ALBA Synchrotron Light Source, E-08290 Cerdanyola del Valles, Spain*
[9]*Institut für Festkörper- und Materialphysik, Technische Universität Dresden, D-01062 Dresden, Germany*
[10]*Van der Waals – Zeeman Institute, IoP, University of Amsterdam, NL-1098 XH Amsterdam, The Netherlands*

Inducing a magnetic gap at the Dirac point of the topological surface state (TSS) in a three-dimensional (3D) topological insulator (TI) is a route to dissipationless charge and spin currents. Ideally, magnetic order is present only at the surface, as through proximity of a ferromagnetic (FM) layer. However, experimental evidence of such a proximity-induced Dirac mass gap is missing, likely due to an insufficient overlap of TSS and the FM subsystem. Here, we take a different approach, namely ferromagnetic extension (FME), using a thin film of the 3D TI Bi_2Te_3, interfaced with a monolayer of the lattice-matched van der Waals ferromagnet $MnBi_2Te_4$. Robust 2D ferromagnetism with out-of-plane anisotropy and a critical temperature of $T_c \approx 15$ K is demonstrated by x-ray magnetic dichroism and electrical transport measurements. Using angle-resolved photoelectron spectroscopy, we observe the opening of a sizable magnetic gap in the 2D FM phase, while the surface remains gapless in the paramagnetic phase above T_c. Ferromagnetic extension paves the way to explore the interplay of strictly 2D magnetism and topological surface states, providing perspectives for realizing robust quantum anomalous Hall and chiral Majorana states.

Engineering the surface of a topological insulator (TI) to host ferromagnetism is expected to enable unconventional phenomena, including topological magnetoelectric effects and Majorana-fermion quasiparticles, with potential applications ranging from spintronics to quantum computation [1–3]. A paradigmatic scenario to achieve this is to interface the TI with a ferromagnetic (FM) layer, aiming to induce an exchange gap in the surface Dirac cone through magnetic proximity while preserving the bulk topology [4]. However, although various FM-TI heterostructures have been investigated [5–12], a clear observation of magnetic topological behavior in such

systems remains elusive. In particular, a direct measurement of a magnetic gap in the surface state is lacking. These difficulties likely arise from a weak hybridization at the FM-TI interface [3,13–15], inhibiting sizable effects on the topological surface state (TSS).

At the same time, it has been proposed that suitable van der Waals (vdW) heterostructures, with weak potential modulation at the interface, may allow the TSS wave function to relocate from the TI surface into the adjacent magnetic layer. Such a ferromagnetic extension (FME) is expected to dramatically enhance the magnetic gap compared to a mere proximity effect [16]. In this Letter we explore the magnetic and topological properties of an epitaxial vdW heterostructure consisting of the TI Bi_2Te_3 and a monolayer $MnBi_2Te_4$ [17]. The structural and chemical similarity of the two compounds has been predicted to generate a FME of Bi_2Te_3 [16]. As schematically shown in Fig. 1(a), the FME is expected to break global time-reversal symmetry (TRS) at the surface, allowing for the opening of a magnetic gap in the TSS below T_c [4]. However, previous experimental attempts to realize a FME could not demonstrate a correlation between electronic structure and magnetic order [10,18–20].

*Celso.Fornari@physik.uni-wuerzburg.de

†Hendrik.Bentmann@ntnu.no; Present address: Center for Quantum Spintronics, Department of Physics, NTNU Norwegian University of Science and Technology, NO-7491 Trondheim, Norway.
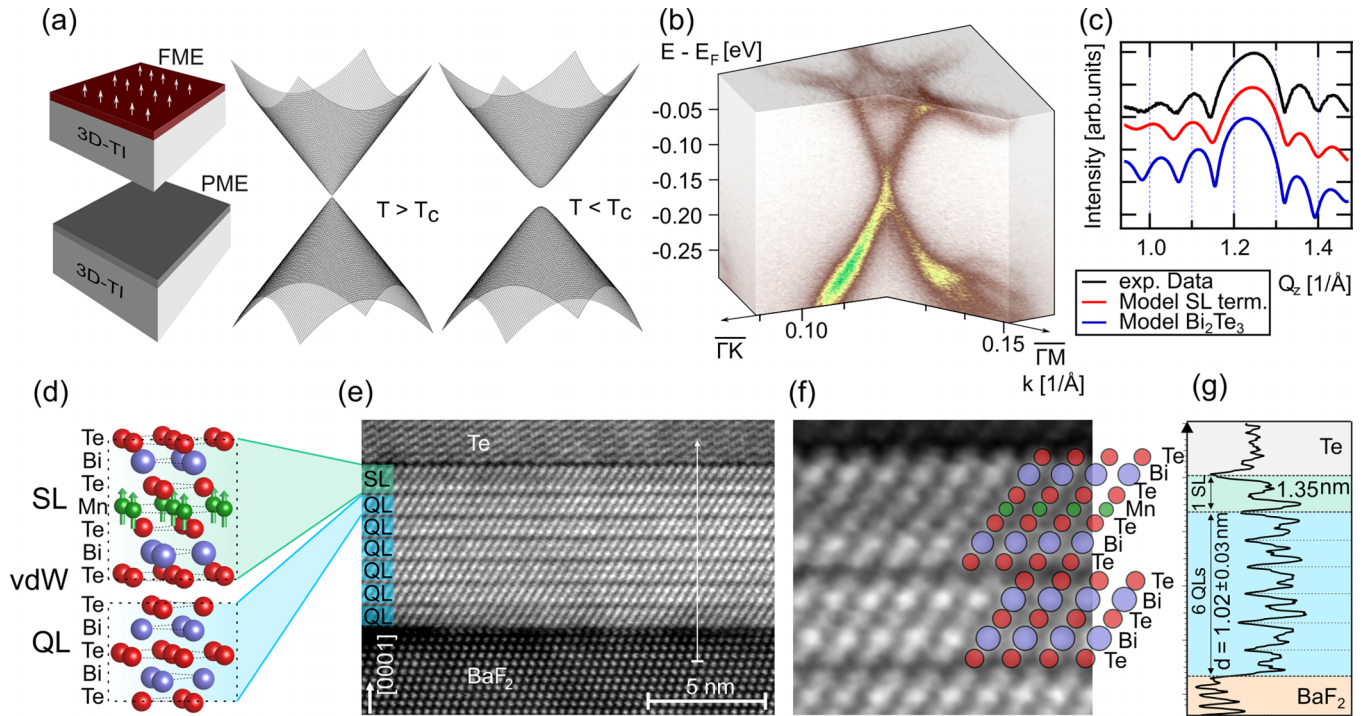
FIG. 1. (a) Scheme of a magnetically extended 3D TI in the ferro- (FME) and paramagnetic (PME) cases. Below T_c, ferromagnetic order in the out-of-plane direction induces a magnetic gap in the topological surface state. (b) 3D ARPES data set of the topological surface state, measured above T_c at $T = 20$ K using p-polarized light at $h\nu = 12$ eV. (c) X-ray diffraction Q_z scan around the (0006) Bragg peak of Bi_2Te_3. The line-shape asymmetry is attributed to the single $MnBi_2Te_4$ layer, as confirmed by calculations. (d) Schematic of the layer structure. The 3D TI Bi_2Te_3 is terminated by a single layer of $MnBi_2Te_4$ containing the magnetically active Mn atomic sheet. (e), (f) Cross-sectional STEM image revealing the sample layer stacking: BaF_2 (111) substrate, 6 quintuple-layer Bi_2Te_3 film, single septuple-layer (SL) $MnBi_2Te_4$, and Te-capping layer. (g) Intensity profile analysis along the trace shown in (e).

We used molecular beam epitaxy to grow a single monolayer $MnBi_2Te_4$ on an epitaxial Bi_2Te_3 layer, as confirmed by high-resolution x-ray diffraction (XRD) and scanning transmission electron microscopy (STEM). X-ray absorption (XAS) and x-ray magnetic circular dichroism (XMCD) were measured at the BOREAS beamline at the ALBA synchrotron in Barcelona. Angle-resolved photoemission spectroscopy (ARPES) measurements were performed at the 1^3 endstation at the BESSY II synchrotron in Berlin. Details of the film growth and characterization methods are presented in the Supplemental Material (SM) [21]. Figure 1(e) shows a cross-section STEM image of a heterostructure. The films are grown on insulating BaF_2 (111) substrates and capped with a Te protective layer to avoid surface oxidation. The vdW gaps parallel to the surface are clearly observed, evidencing the formation of high-quality layers and the absence of twinned domains (Fig. S4 [21]). A single $MnBi_2Te_4$ septuple layer (SL) is present on the surface, as verified by the zoom-in STEM image in Fig. 1(f). The difference in contrast allows us to distinguish the three elements on their respective sites. Figure 1(g) shows a line profile extracted along the [0001] direction [white arrow in Fig. 1(e)]. We obtain an average thickness of 1.02(3) nm for the quintuple layers (QLs) and of 1.35 nm for the SL, consistent with values reported for the individual compounds [36,37]. In Fig. 1(c) we compare an experimental Q_z XRD scan, recorded around the Bi_2Te_3 (0006) Bragg peak, with simulated scans for Bi_2Te_3 with and without an additional SL of $MnBi_2Te_4$. The experimental

line shape shows a pronounced asymmetry with a shoulder at lower Q_z, which, based on our XRD simulations (see Fig. S5 [21] for details), can be assigned to the presence of a single $MnBi_2Te_4$ SL.

Figure 1(b) shows ARPES data near the Fermi level (E_F) along the high-symmetry directions. The data were obtained in the paramagnetic regime of the $MnBi_2Te_4$ layer above T_c (cf. Figs. 2 and 3). A TSS with a Dirac-like band dispersion is observed, as further confirmed by the photon-energy-dependent data in Fig. S9. Interestingly, the TSS dispersion is strongly modified from the one of a pristine Bi_2Te_3 (0001) surface [38]. In agreement with theoretical calculations [16], the Dirac point is shifted upwards in energy into the bulk band gap. As a result, both the upper and lower parts of the Dirac cone display a linear dispersion near the $\bar{\Gamma}$ point, in contrast to Bi_2Te_3 (0001). Moreover, the Fermi surface acquires a pronounced hexagonal star shape with cusps along $\overline{\Gamma M}$, in accordance with recent calculations [20]. The strong effect of the $MnBi_2Te_4$ single layer on the TSS band dispersion and the overall agreement with calculations support a scenario where the TSS wave function relocates into the SL, as predicted theoretically [16].

We now demonstrate the presence of ferromagnetism in the $MnBi_2Te_4$ monolayer, employing x-ray magnetic circular dichroism (XMCD) and electrical transport. The data were collected in total-electron-yield mode with light incidence and external field oriented along the surface normal. Figure 2(a) shows x-ray absorption (XAS) and XMCD data in saturation
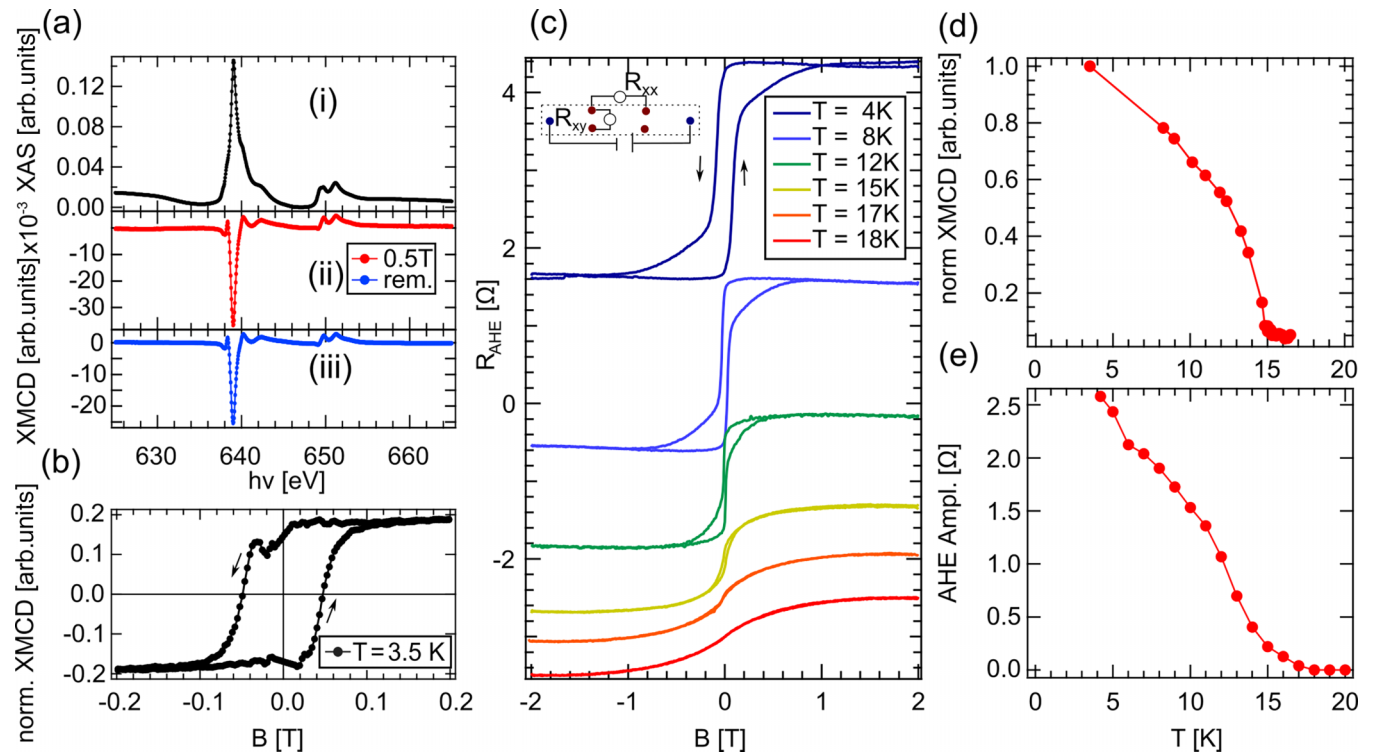
FIG. 2. (a) XAS and XMCD data confirming a stable ferromagnetic state of MnBi$_2$Te$_4$. (i) XAS data set at the Mn $L_{2,3}$ edge. (ii), (iii) XMCD difference spectra at $T = 3.5$ K for a saturation field of 0.5 T and in remanence. (b) XMCD hysteresis at the same temperature indicating long-range ferromagnetic order. (c) Anomalous Hall effect (AHE) in a single-layer MnBi$_2$Te$_4$/Bi$_2$Te$_3$ heterostructure vs magnetic field, at several temperatures. The arrows indicate the magnetic field sweep direction. Curves are vertically shifted for clarity. A clear hysteretic behavior of the AHE is observed below 18 K, with coercive fields up to 90 mT, confirming the ferromagnetic behavior of the single MnBi$_2$Te$_4$ layer. The inset shows a schematic of the pseudo-Hall bar geometry of the transport experiments. (d) Temperature dependence of the remnant XMCD signal yielding a critical temperature of 14.9 K. (e) Temperature dependence of the AHE amplitude at zero field extracted from the data in (c).

and in remanence. The XAS line shape of the Mn $L_{2,3}$ absorption edge strongly resembles the one of bulk MnBi$_2$Te$_4$ [17], indicating Mn ions in the same oxidation state. The apparent absence of Mn oxide components in the spectra further verifies the successful preparation of pristine surfaces through the mechanical removal of the Te cap, as established earlier for Bi$_2$Te$_3$ [39]. As seen from the XMCD signals in saturation and remanence, the MnBi$_2$Te$_4$ monolayer hosts a stable ferromagnetic state at the lowest measured temperature of $\sim$3.5 K, with a remanent XMCD of $(87.5 \pm 1.5)\%$ as compared to the saturated signal. The field-dependent Mn XMCD signal in Fig. 2(b) shows an open hysteresis loop with a coercive field of -48 mT and a pronounced saturation behavior above 100 mT in the FM phase. The approximate square shape of the hysteresis indicates an out-of-plane easy axis, as further confirmed by measurements in in-plane geometry (see Fig. S7 [21]). Following the temperature dependence of the remnant XMCD signal in Fig. 2(d), a reduction of the remnant magnetization towards a critical temperature of $\sim$14.9 K is observed. The decay towards T_c is well described by a critical exponent of $\beta = 0.484$ (see Fig. S8 [21]).

To investigate the global magnetic properties we performed magnetotransport measurements. For these experiments thinner Bi$_2$Te$_3$ epilayers (3 QLs) were employed to minimize contributions from nonmagnetic Bi$_2$Te$_3$ to the charge transport. The samples were covered *in situ*, after growth, by

a 30-nm-thick BaF$_2$ capping layer to avoid surface contamination and oxidation during air exposure (see SM [21] for more detailed information). We contacted a macroscopic millimeter-scale as-grown thin film in a pseudo-Hall bar geometry. The inset in Fig. 2(c) shows a schematic of the geometry for Hall and longitudinal configurations, where the current is applied through the bar while measuring the resistance perpendicular and parallel to the current, respectively (see also Fig. S6 [21]). Figure 2(c) displays data of Hall measurements performed with perpendicular magnetic fields at different temperatures from 4 to 20 K, after subtraction of the linear normal Hall-effect background. We observe a pronounced anomalous Hall-effect (AHE) hysteresis at 4 K with an amplitude of 2.8 Ω. Further, at 4 K, the coercive field reaches 90 mT, and decreases above 10 K (10 mT). In Fig. 2(e), the AHE hysteresis amplitude is extracted from the anomalous Hall curves. The amplitude of the hysteresis decreases with increasing temperature and the loop finally vanishes, pointing to a critical temperature of $\sim$17 K, comparable to the one observed in XMCD. Since the Bi$_2$Te$_3$ epilayer is nonmagnetic and given the XMCD data, the AHE hysteresis can be attributed to the MnBi$_2$Te$_4$ monolayer.

Hence, our results from these two complementary probes establish a FM state in monolayer MnBi$_2$Te$_4$/Bi$_2$Te$_3$ with a T_c of 15 ± 2 K and out-of-plane anisotropy (see Fig. S7 [21]). This refutes earlier claims of paramagnetic properties
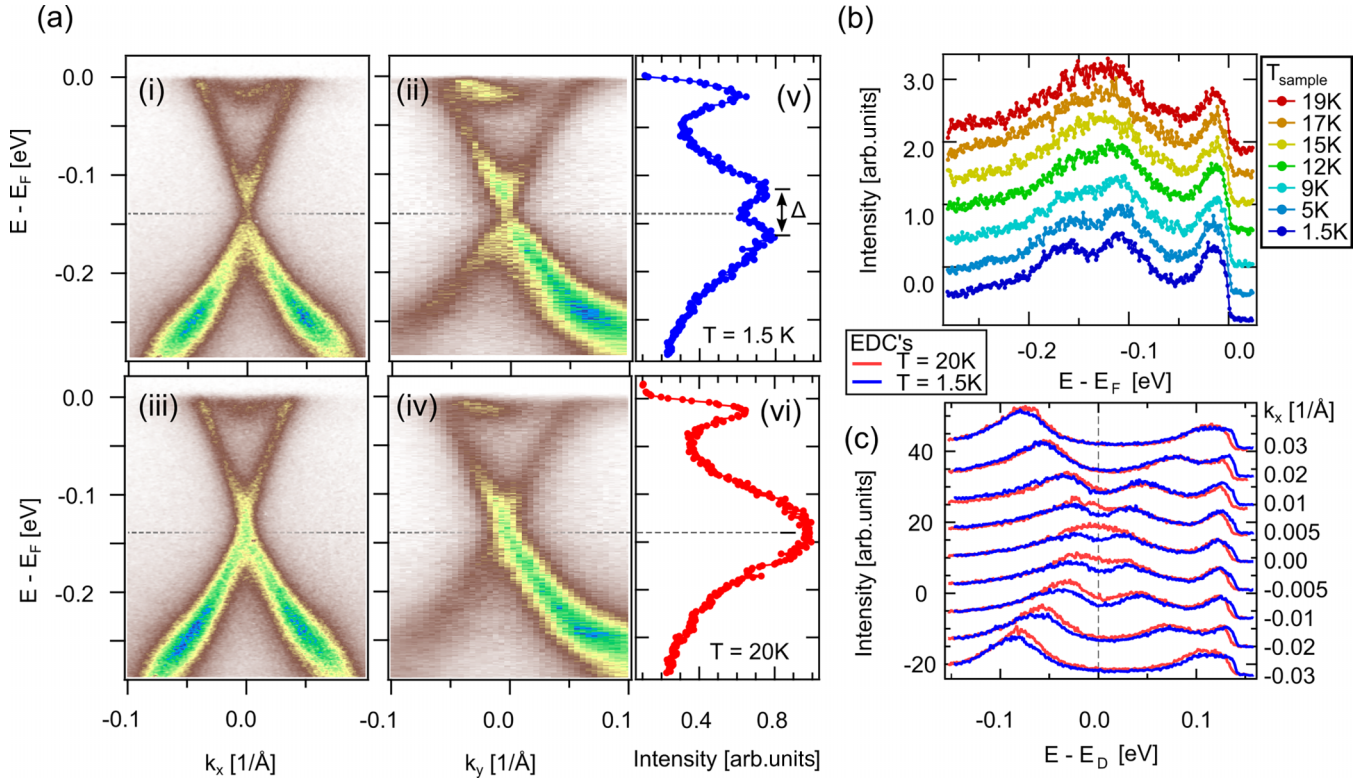
FIG. 3. (a) ARPES data acquired below (top row) and above (bottom row) the critical temperature T_c using p-polarized light at $h\nu = 12$ eV. Data sets acquired perpendicular [(i) and (iii)] and along [(ii) and (iv)] the plane of incidence are shown. (v) and (vi) display energy distribution curves (EDC) at the the $\bar{\Gamma}$ point, revealing a magnetic exchange splitting at the Dirac point below T_c. (b) Temperature-dependent EDC at the $\bar{\Gamma}$ point, showing the spectral-weight evolution across T_c. (c) Momentum-dependent EDC above and below T_c, taken from the data sets in (a). The energy scales are relative to the respective Dirac-point position, to compensate for a small temperature-dependent energy shift. The ferromagnetic order affects the spectral weight predominantly in a narrow momentum range of $\delta k = \pm 0.01$ Å^{-1} around the $\bar{\Gamma}$ point.

at lower temperatures [19], but is in line with theoretical predictions [16] and experimental results for thin MnBi$_2$Te$_4$ flakes exfoliated from bulk crystals [40]. Our magnetic data also vastly deviate from a recent work [20], where the growth of monolayer MnBi$_2$Te$_4$/Bi$_2$Te$_3$ was claimed without appropriate evidence from structural data.

We next discuss the temperature dependence of the TSS dispersion across T_c of the MnBi$_2$Te$_4$ monolayer. As schematically shown in Fig. 1(a), an out-of-plane FM layer at the surface of a 3D TI is expected to break TRS, lifting the topological protection and allowing for a gap to open at the Dirac point. In Fig. 3(a) we present high-resolution ARPES measurements of the TSS along k_x and k_y for temperatures well above and below T_c, acquired with a photon energy of $h\nu = 12$ eV. To exclude angular misalignment, the ARPES intensity around the $\bar{\Gamma}$ point is sampled in small increments along both $k_{\parallel}$ components. The rather pronounced intensity asymmetry along k_y arises from the experimental geometry, with p-polarized light incident in the yz plane.

The ARPES data acquired below T_c ($T = 1.5$ K) reveal a reduction of spectral weight at the Dirac point, i.e., at around -0.14 eV, and a splitting into two peak components at $\bar{\Gamma}$, as directly visible in the energy distribution curve (EDC) [Fig. 3(a)]. By contrast, the spectral-weight reduction and the splitting disappear above T_c ($T = 20$ K), demonstrating their magnetic origin. We determine an exchange splitting of $\Delta = 35$ meV at $T = 1.5$ K (see Fig. S12 [21]), which corresponds

to the size of the gap in the TSS and is in good agreement with theory [16].

The temperature series in Fig. 3(b) shows how the spectral-weight distribution of the TSS at $\bar{\Gamma}$ evolves as the temperature is varied across T_c. With increasing temperature the double-peak structure gradually becomes less well defined but remains observable in the FM regime, up to 12 K. At and above $T_c \sim 15$ K, the spectra differ qualitatively from the FM regime, showing a single maximum, a rather symmetric line shape, and no discernible double-peak structure or peak shoulder. Hence, the data indicate a closing of the magnetic gap at T_c, as expected from our XMCD experiments that show a vanishing net magnetization m_z and thus a globally preserved TRS. The temperature-dependent line shape in Fig. 3(b) can be modeled by a photoemission toy model taking into account experimental broadening. The size of the magnetic exchange gap extracted in this way can be seen match the power-law dependence in the form of $\Delta(T) = \Delta_0(1 - T/T_c)^{\beta}$, with $\beta = 0.484$ as estimated from the XMCD data (see Figs. S8 and S12 [21]). Hence, our combined XMCD and ARPES results support an approximate relation $\Delta \propto m_z$. The origin of the gap can therefore be attributed to the FM order at the surface.

To study the momentum-dependent effect of m_z on the TSS dispersion, we consider a more detailed comparison of the ARPES data near the $\bar{\Gamma}$ point above and below T_c [Fig. 3(c)]. It is evident from the data that the FM order affects the

dispersion only in a narrow $k_\parallel$ range of about ± 0.01 Å^{-1}. At larger momenta the dispersion remains largely unchanged. This observation is in line with an effective model for a TSS perturbed by an exchange field m_z [4], described by $H = v_F(\sigma_x k_y - \sigma_y k_x) + m_z \sigma_z$. The ratio m_z/v_F, quantifying the relative strengths of exchange interaction and spin-orbit interaction, provides a natural scale δk on which m_z modifies the TSS dispersion and wave function which we estimate to ± 0.01 Å^{-1}.

Taken together, we demonstrate how a strictly 2D ferromagnetic state induces a robust gap at the surface of a 3D topological insulator. Preserving the bulk topological properties, this situation overcomes the previous paradigm of 3D magnetic topological insulators where time-reversal symmetry is broken in the entire bulk [2,3,17,41–43]. Following theoretical predictions [16], our results establish ferromagnetic extension as a distinct phenomenon in the surface and interface physics of topological insulators, which can be exploited in device concepts.

Signatures of a magnetic gap were previously also found in cleaved $MnBi_8Te_{13}$ bulk crystals [43] and randomly stacked $MnBi_2Te_4/Bi_2Te_3$ bulk layers [41]. However, these systems are not available in thin-film form, and their surfaces display spatially inhomogeneous structural termination, electronic properties, and magnetic gaps [43]. By contrast, ferromagnetically extended Bi_2Te_3 paves the way to systematically explore magnetic topological phenomena in complex heterostructures and the interplay of topology and 2D magnetism.

In particular, monolayer $MnBi_2Te_4/Bi_2Te_3$ introduces a textbooklike quantum anomalous Hall (QAH) system, consisting of a genuine bulk 3D TI and a magnetically gapped surface [4]. Moreover, the prospect of independently manipulating the magnetic states of the two opposing surfaces in a SL-$MnBi_2Te_4/Bi_2Te_3/$SL-$MnBi_2Te_4$ heterostructure, e.g., through proximity to adjacent magnetic layers [44], could

facilitate the study of axion-insulator behavior [45] or of the recently discovered layer Hall effect [46]. This is different from thin $MnBi_2Te_4$ flakes where fine tuning of the layer thickness is required to achieve an uncompensated or compensated antiferromagnetic state [42,46,47].

The strictly 2D magnetic state may further allow for integration into advanced heterostructures to explore more exotic topological properties. For example, SL-$MnBi_2Te_4/Bi_2Te_3/NbSe_2$ structures were recently predicted as an ideal experimental platform to realize chiral Majorana edge states [48]. $MnBi_2Te_4/CrI_3$ magnetic hybrid structures have been suggested as a route to high Chern number QAH states [44]. Furthermore, we note that SL-$MnBi_2Te_4/Bi_2Te_3$ constitutes an example of a 2D monolayer van der Waals magnet that hosts a topological surface state, which opens different research directions in the field of 2D magnetism [49]. Among others, it offers the intriguing opportunity to investigate the influence of topological surface electrons on a truly 2D ferromagnetic state [50,51].

[1] B. A. Bernevig, C. Felser, and H. Beidenkopf, Progress and prospects in magnetic topological materials, Nature (London) **603**, 41 (2022).

[2] C.-Z. Chang, J. Zhang, X. Feng, J. Shen, Z. Zhang, M. Guo, K. Li, Y. Ou, P. Wei, L.-L. Wang *et al.*, Experimental observation of the quantum anomalous Hall effect in a magnetic topological insulator, Science **340**, 167 (2013).

[3] Y. Tokura, K. Yasuda, and A. Tsukazaki, Magnetic topological insulators, Nat. Rev. Phys. **1**, 126 (2019).

[4] X.-L. Qi and S.-C. Zhang, Topological insulators and superconductors, Rev. Mod. Phys. **83**, 1057 (2011).

[5] L. A. Wray, S.-Y. Xu, Y. Xia, D. Hsieh, A. V. Fedorov, Y. San Hor, R. J. Cava, A. Bansil, H. Lin, and M. Z. Hasan, A topological insulator surface under strong Coulomb, magnetic and disorder perturbations, Nat. Phys. **7**, 32 (2011).

[6] M. R. Scholz, J. Sánchez-Barriga, D. Marchenko, A. Varykhalov, A. Volykhov, L. V. Yashina, and O. Rader, Tolerance of Topological Surface States towards Magnetic Moments: Fe on Bi_2Se_3, Phys. Rev. Lett. **108**, 256810 (2012).

[7] M. Lang, M. Montazeri, M. C. Onbasli, X. Kou, Y. Fan, P. Upadhyaya, K. Yao, F. Liu, Y. Jiang, W. Jiang *et al.*, Proximity induced high-temperature magnetic order in topological insulator-ferrimagnetic insulator heterostructure, Nano Lett. **14**, 3459 (2014).

[8] C. Tang, C.-Z. Chang, G. Zhao, Y. Liu, Z. Jiang, C.-X. Liu, M. R. McCartney, D. J. Smith, T. Chen, J. S. Moodera *et al.*, Above 400-K robust perpendicular ferromagnetic phase in a topological insulator, Sci. Adv. **3**, e1700307 (2017).

[9] F. Katmis, V. Lauter, F. S. Nogueira, B. A. Assaf, M. E. Jamer, P. Wei, B. Satpati, J. W. Freeland, I. Eremin, D. Heiman *et al.*, A high-temperature ferromagnetic topological insulating phase by proximity coupling, Nature (London) **533**, 513 (2016).

[10] T. Hirahara, M. M. Otrokov, T. Sasaki, K. Sumida, Y. Tomohiro, S. Kusaka, Y. Okuyama, S. Ichinokura, M. Kobayashi, Y. Takeda *et al.*, Fabrication of a novel magnetic topological heterostructure and temperature evolution of its massive Dirac cone, Nat. Commun. **11**, 4821 (2020).

[11] C. Lee, F. Katmis, P. Jarillo-Herrero, J. S. Moodera, and N. Gedik, Direct measurement of proximity-induced magnetism at the interface between a topological insulator and a ferromagnet, Nat. Commun. **7**, 12014 (2016).

[12] M. Mogi, T. Nakajima, V. Ukleev, A. Tsukazaki, R. Yoshimi, M. Kawamura, K. S. Takahashi, T. Hanashima, K. Kakurai, T.-h. Arima, M. Kawasaki, and Y. Tokura, Large Anomalous Hall Effect in Topological Insulators with Proximitized Ferromagnetic Insulators, Phys. Rev. Lett. **123**, 016804 (2019).

[13] A. I. Figueroa, F. Bonell, M. G. Cuxart, M. Valvidares, P. Gargiani, G. van der Laan, A. Mugarza, and S. O. Valenzuela, Absence of Magnetic Proximity Effect at the Interface of Bi_2Se_3 and $(Bi, Sb)_2Te_3$ with EuS, Phys. Rev. Lett. **125**, 226801 (2020).

[14] L. J. Riddiford, A. J. Grutter, T. Pillsbury, M. Stanley, D. Reifsnyder Hickey, P. Li, N. Alem, N. Samarth, and Y. Suzuki, Understanding Signatures of Emergent Magnetism in Topological Insulator/Ferrite Bilayers, Phys. Rev. Lett. **128**, 126802 (2022).

[15] S. Eremeev, V. Men'shov, V. Tugushev, and E. V. Chulkov, Interface induced states at the boundary between a 3D topological insulator Bi_2Se_3 and a ferromagnetic insulator EuS, J. Magn. Magn. Mater. **383**, 30 (2015).

[16] M. M. Otrokov, T. V. Menshchikova, M. G. Vergniory, I. P. Rusinov, A. Y. Vyazovskaya, Y. M. Koroteev, G. Bihlmayer, A. Ernst, P. M. Echenique, A. Arnau *et al.*, Highly-ordered wide bandgap materials for quantized anomalous Hall and magneto-electric effects, 2D Mater. **4**, 025082 (2017).

[17] M. M. Otrokov, I. I. Klimovskikh, H. Bentmann, D. Estyunin, A. Zeugner, Z. S. Aliev, S. Gaß, A. U. B. Wolter, A. V. Koroleva, A. M. Shikin *et al.*, Prediction and observation of an antiferromagnetic topological insulator, Nature (London) **576**, 416 (2019).

[18] T. Hirahara, S. V. Eremeev, T. Shirasawa, Y. Okuyama, T. Kubo, R. Nakanishi, R. Akiyama, A. Takayama, T. Hajiri, S.-I. Ideta *et al.*, Large-gap magnetic topological heterostructure formed by subsurface incorporation of a ferromagnetic layer, Nano Lett. **17**, 3493 (2017).

[19] T. Fukasawa, S. Kusaka, K. Sumida, M. Hashizume, S. Ichinokura, Y. Takeda, S. Ideta, K. Tanaka, R. Shimizu, T. Hitosugi, and T. Hirahara, Absence of ferromagnetism in $MnBi_2Te_4/Bi_2Te_3$ down to 6 K, Phys. Rev. B **103**, 205405 (2021).

[20] Q. Li, C. X. Trang, W. Wu, J. Hwang, D. Cortie, N. Medhekar, S.-K. Mo, S. A. Yang, and M. T. Edmonds, Large magnetic gap in a designer ferromagnet-topological insulator-ferromagnet heterostructure, Adv. Mater. **34**, 2107520 (2022).

[21] See Supplemental Material at http://link.aps.org/supplemental/10.1103/PhysRevResearch.5.L022019 for detailed information on the sample preparation and data treatment, which includes Refs. [22–35].

[22] O. Caha *et al.*, Growth, structure, and electronic properties of epitaxial bismuth telluride topological insulator films on BaF_2 (111) substrates, Cryst. Growth Des. **13**, 3365 (2013).

[23] C. Fornari, P. Rappl, S. Morelhão, and E. Abramof, Structural defects and electronic phase diagram of topological insulator bismuth telluride epitaxial films, J. Appl. Phys. **119**, 165303 (2016).

[24] C. Fornari *et al.*, Structural properties of Bi_2Te_3 topological insulator thin films grown by molecular beam epitaxy on (111) BaF_2 substrates, Mater. Res. Express **5**, 116410 (2018).

[25] P. Kagerer *et al.*, Molecular beam epitaxy of antiferromagnetic $(MnBi_2Te_4)(Bi_2Te_3)$ thin films on BaF_2 (111), J. Appl. Phys. **128**, 135303 (2020).

[26] J. Dai, W. Wang, M. Brahlek, N. Koirala, M. Salehi, S. Oh, and W. Wu, Restoring pristine Bi_2Se_3 surfaces with an effective Se decapping process, Nano Res. **8**, 1222 (2015).

[27] M. Björck and G. Andersson, GenX: an extensible x-ray reflectivity refinement program utilizing differential evolution, J. Appl. Crystallogr. **40**, 1174 (2007).

[28] R. Penacchio *et al.*, Statistical modeling of epitaxial thin films of an intrinsic antiferromagnetic topological insulator, Thin Solid Films **750**, 139183 (2022).

[29] A. Barla *et al.*, Design and performance of BOREAS, the beamline for resonant X-ray absorption and scattering experiments at the ALBA synchrotron light source, J. Synchrotron Radiat. **23**, 1507 (2016).

[30] S. Grauer, K. M. Fijalkowski, S. Schreyeck, M. Winnerlein, K. Brunner, R. Thomale, C. Gould, and L. W. Molenkamp, Scaling of the Quantum Anomalous Hall Effect as an Indicator of Axion Electrodynamics, Phys. Rev. Lett. **118**, 246801 (2017).

[31] T. R. Peixoto *et al.*, Non-local effect of impurity states on the exchange coupling mechanism in magnetic topological insulators, npj Quantum Mater. **5**, 87 (2020).

[32] A. Bedoya-Pinto *et al.*, Intrinsic 2D-XY ferromagnetism in a van der Waals monolayer, Science **374**, 616 (2021).

[33] Y. J. Chen, L. X. Xu, J. H. Li, Y. W. Li, H. Y. Wang, C. F. Zhang, H. Li, Y. Wu, A. J. Liang, C. Chen *et al.*, Topological Electronic Structure and its Temperature Evolution in Antiferromagnetic Topological Insulator $MnBi_2Te_4$, Phys. Rev. X **9**, 041040 (2019).

[34] Y. J. Hao, P. Liu, Y. Feng, X. M. Ma, E. F. Schwier, M. Arita, S. Kumar, C. Hu, R. Lu, M. Zeng *et al.*, Gapless Surface Dirac Cone in Antiferromagnetic Topological Insulator $MnBi_2Te_4$, Phys. Rev. X **9**, 041038 (2019).

[35] R. C. Vidal, H. Bentmann, J. I. Facio, T. Heider, P. Kagerer, C. I. Fornari, T. R. F. Peixoto, T. Figgemeier, S. Jung, C. Cacho *et al.*, Orbital Complexity in Intrinsic Magnetic Topological Insulators $MnBi_4Te_7$ and $MnBi_6Te_{10}$, Phys. Rev. Lett. **126**, 176403 (2021).

[36] A. Zeugner, F. Nietschke, A. U. Wolter, S. Gaß, R. C. Vidal, T. R. Peixoto, D. Pohl, C. Damm, A. Lubk, R. Hentrich *et al.*, Chemical aspects of the candidate antiferromagnetic topological insulator $MnBi_2Te_4$, Chem. Mater. **31**, 2795 (2019).

[37] S. L. Morelhão, C. I. Fornari, P. H. O. Rappl, and E. Abramof, Nanoscale characterization of bismuth telluride epitaxial layers by advanced x-ray analysis, J. Appl. Crystallogr. **50**, 399 (2017).

[38] Y. L. Chen, J. G. Analytis, J.-H. Chu, Z. K. Liu, S.-K. Mo, X. L. Qi, H. J. Zhang, D. H. Lu, X. Dai, Z. Fang, S. C. Zhang, I. R. Fisher, Z. Hussain, and Z.-X. Shen, Experimental realization of a three-dimensional topological insulator, Bi_2Te_3, Science **325**, 178 (2009).

[39] C. I. Fornari, P. H. O. Rappl, S. L. Morelhão, T. R. F. Peixoto, H. Bentmann, F. Reinert, and E. Abramof, Preservation of pristine Bi_2Te_3 thin film topological insulator surface after *ex situ* mechanical removal of Te capping layer, APL Mater. **4**, 106107 (2016).

[40] S. Yang, X. Xu, Y. Zhu, R. Niu, C. Xu, Y. Peng, X. Cheng, X. Jia, Y. Huang, X. Xu, J. Lu, and Y. Ye, Odd-Even Layer-Number Effect and Layer-Dependent Magnetic Phase Diagrams in $MnBi_2Te_4$, Phys. Rev. X **11**, 011003 (2021).

[41] E. D. Rienks, S. Wimmer, J. Sánchez-Barriga, O. Caha, P. S. Mandal, J. Růžička, A. Ney, H. Steiner, V. V. Volobuev, H. Groiß *et al.*, Large magnetic gap at the Dirac point in

Bi$_2$Te$_3$/MnBi$_2$Te$_4$ heterostructures, Nature (London) **576**, 423 (2019).

[42] Y. J. Deng, Y. J. Yu, M. Z. Shi, Z. X. Guo, Z. H. Xu, J. Wang, X. H. Chen, and Y. B. Zhang, Quantum anomalous Hall effect in intrinsic magnetic topological insulator MnBi$_2$Te$_4$, Science **367**, 895 (2020).

[43] R. Lu, H. Sun, S. Kumar, Y. Wang, M. Gu, M. Zeng, Y.-J. Hao, J. Li, J. Shao, X.-M. Ma *et al.*, Half-Magnetic Topological Insulator with Magnetization-Induced Dirac Gap at a Selected Surface, Phys. Rev. X **11**, 011039 (2021).

[44] H. Fu, C.-X. Liu, and B. Yan, Exchange bias and quantum anomalous Hall effect in the MnBi$_2$Te$_4$/CrI$_3$ heterostructure, Sci. Adv. **6**, eaaz0948 (2020).

[45] K. Nomura and N. Nagaosa, Surface-Quantized Anomalous Hall Current and the Magnetoelectric Effect in Magnetically Disordered Topological Insulators, Phys. Rev. Lett. **106**, 166802 (2011).

[46] A. Gao, Y.-F. Liu, C. Hu, J.-X. Qiu, C. Tzschaschel, B. Ghosh, S.-C. Ho, D. Bérubé, R. Chen, H. Sun *et al.*, Layer Hall effect in a 2D topological axion antiferromagnet, Nature (London) **595**, 521 (2021).

[47] C. Liu, Y. Wang, H. Li, Y. Wu, Y. Li, J. Li, K. He, Y. Xu, J. Zhang, and Y. Wang, Robust axion insulator and Chern insulator phases in a two-dimensional antiferromagnetic topological insulator, Nat. Mater. **19**, 522 (2020).

[48] X. Zhang and F. Liu, Prediction of Majorana edge states from magnetized topological surface states, Phys. Rev. B **103**, 024405 (2021).

[49] M. Gibertini, M. Koperski, A. F. Morpurgo, and K. S. Novoselov, Magnetic 2D materials and heterostructures, Nat. Nanotechnol. **14**, 408 (2019).

[50] Q. Liu, C.-X. Liu, C. Xu, X.-L. Qi, and S.-C. Zhang, Magnetic Impurities on the Surface of a Topological Insulator, Phys. Rev. Lett. **102**, 156603 (2009).

[51] M. Scholten, J. I. Facio, R. Ray, I. M. Eremin, J. van den Brink, and F. S. Nogueira, Finite temperature fluctuation-induced order and responses in magnetic topological insulators, Phys. Rev. Res. **3**, L032014 (2021).